Effects of Alkyl Substitution on the Energetics of Enolate Anions and Radicals

Leah S. Alconcel, Hans-Jürgen Deyerl,† and Robert E. Continetti*

Contribution from the Department of Chemistry and Biochemistry-0340, University of California, San Diego, 9500 Gilman Drive, La Jolla, California 92093-0340

Received August 24, 2001

Abstract: The photoelectron spectra of the structural isomers of the three- and four-carbon enolate anions, *n*-$C_3H_5O^-$, *i*-$C_3H_5O^-$, *n*-$C_4H_7O^-$, *s*-$C_4H_7O^-$, and *i*-$C_4H_7O^-$ have been measured at 355 nm. Both the X(^{2}A″) ground and A(^{2}A′) first excited states of the corresponding radicals were accessed from the X(^{1}A′) ground state of the enolate anions. The separation energies of the ground and first excited states (T_0) were determined: T_0[(*E*)-*n*-C_3H_5O] = 1.19 ± 0.02 eV, T_0[(*Z*)-*n*-C_3H_5O] = 0.99 ± 0.02 eV, T_0[*i*-C_3H_5O] = 1.01 ± 0.02 eV, T_0[*n*-C_4H_7O] = 1.19 ± 0.02 eV, T_0[(2,3)-*s*-C_4H_7O] = 1.25 ± 0.02 eV, T_0[(1,2)-*s*-C_4H_7O] = 0.98 ± 0.02 eV, and T_0[*i*-C_4H_7O] = 1.36 ± 0.02 eV. The effects of alkyl substitution on the vibronic structure and energetics previously observed in the vinoxy radical are discussed. The X(^{1}A′)−X(^{2}A″) relative stability is strongly influenced by substitution whereas the X(^{1}A′)−A(^{2}A′) relative stability remains nearly constant for all of the observed structural isomers. Alkyl substitution at the carbonyl carbon affects vibronic structure more profoundly than the energetics, while the converse is observed upon alkyl substitution at the α carbon.

1. Introduction

The involvement of enolate and alkoxy radicals and anions as intermediates in photochemical smog cycles, combustion reactions, and many organic syntheses of complex compounds has prompted a number of spectroscopic studies.[1−3] Recently, the dependence of the energetics and vibronic activity on the branching and number of carbons in alkoxy radicals has been studied.[4,5] The identification of such trends provides a tool for predicting the photoreactive properties of these important classes of compounds. In this laboratory, the effects of alkyl substitution on the properties of enolates were studied, extending previous experimental and theoretical work performed on the simplest enolate, the two-carbon species commonly known as vinoxide or acetaldehyde enolate, and the two lowest electronic states of the vinoxy radical.[6] Photodetachment of an electron from the CCO nonbonding π(a″) orbital of vinoxide yields ground X(^{2}A″) state vinoxy and photodetachment from the oxygen σ_{2p}(a′) orbital yields the first excited A(^{2}A′) state. In the neutral, the singly occupied π(a″) orbital can interact with the CCO bonding π(a″) orbital whereas the singly occupied σ_{2p}(a′) orbital cannot, resulting in the large separation energy between the X(^{2}A″) and A(^{2}A′) states, T_0.l,, of 1.015 ± 0.015 eV.

The ground X(^{2}A″) state of the three- and four-carbon enolates has been studied previously through threshold photodetachment and photoelectron spectroscopy and the electron affinities were measured.[7−10] Optically allowed B(^{2}A″) ← X(^{2}A″) transitions in these species have also been studied via laser-induced fluorescence (LIF), yielding fluorescence lifetimes and frequencies of normal vibrational modes in the B and X states.[11−14] The barriers to internal methyl rotation of the three-carbon enolates have been determined with LIF studies combined with ab initio calculations.[13,14]

Most of the structural isomers of the C_3H_5O and C_4H_7O enolate anions exist in more than one constitutional isomeric or stereoisomeric form.[15] The constitutional isomers of *sec*-butyraldehyde enolate were studied by selective deuteration of the 2-butanone precursor to 2-butanone-*3*,*3*-d_2.[7] Following proton abstraction by F^-, the (1,2) and (2,3) forms of the enolate could be distinguished by mass. Efforts have recently been made to study stereoisomeric forms of enolates independently.[10−12,14,16] Ion cyclotron resonance was used to obtain electron photodetachment spectra of the (*E*) and (*Z*) stereoisomers of *n*-propionaldehyde enolate (*n*-C_3H_5O).[10] The electron affinities of (*E*)-*n*-C_3H_5O and (*Z*)-*n*-C_3H_5O were determined to be 1.619 ± 0.007 and 1.73 ± 0.01 eV respectively from this threshold photodetachment study. The preferred orientation of the methyl

* Address correspondence to this author: rcontinetti@ucsd.edu.
† Current address: Research Center COM, DTU, DK-2800 Kgs. Lyngby, Denmark.

(1) Ager, D. J.; East, M. B. *Asymmetric Synthetic Methodology*; CRC Press: Boca Raton, FL, 1996.
(2) Wan, R. L.; Chen, X. R.; Wu, F.; Weiner, B. R. *Chem. Phys. Lett.* **1996**, *260*, 539−544.
(3) Brock, L. R.; Rohlfing, E. A. *J. Chem. Phys.* **1997**, *106*, 10048−10065.
(4) Carter, C. C.; Atwell, J. R.; Gopalakrishnan, S.; Miller, T. A. *J. Phys. Chem. A* **2000**, *104*, 9165−9170.
(5) Carter, C. C.; Gopalakrishnan, S.; Atwell, J. R.; Miller, T. A. *J. Phys. Chem. A* **2001**, *105*, 2925−2928.
(6) Alconcel, L. S.; Deyerl, H.-J.; Zengin, V.; Continetti, R. E. *J. Phys. Chem. A* **1999**, *103*, 9190−9194.
(7) Zimmerman, A. H.; Reed, K. J.; Brauman, J. I. *J. Am. Chem. Soc.* **1977**, *99*, 7203−7209.
(8) Ellison, G. B.; Engelking, P. C.; Lineberger, W. C. *J. Chem. Phys.* **1982**, *86*, 4873−4878.
(9) Brinkman, E. A.; Berger, S.; Marks, J.; Brauman, J. I. *J. Chem. Phys.* **1993**, *99*, 7586−7594.
(10) Romer, B. C.; Brauman, J. I. *J. Am. Chem. Soc.* **1997**, *119*, 2054−2055.
(11) Washida, N.; Inomata, S.; Furubayashi, M. *J. Phys. Chem. A* **1998**, *102*, 7924−7930.
(12) Williams, S.; Zingher, E.; Weisshaar, J. C. *J. Phys. Chem. A* **1998**, *102*, 2297−2301.
(13) Williams, S.; Harding, L. B.; Stanton, J. F.; Weisshaar, J. C. *J. Phys. Chem. A* **2000**, *104*, 10131−10138.
(14) Williams, S.; Harding, L. B.; Stanton, J. F.; Weisshaar, J. C. *J. Phys. Chem. A* **2000**, *104*, 9906−9913.
(15) Squires, R. R.; DePuy, C. H. *Org. Mass Spectrom.* **1982**, *17*, 187−191.

10.1021/ja0120431 CCC: $20.00
Published on Web 00/00/0000 PAGE EST: 6.9

group with respect to the CCO moiety was derived for the *n*-propionaldehyde enolate (*n*-C_3H_5O) and acetone enolate (*i*-C_3H_5O) radical X($^2A''$) and B($^2A''$) states.[13,14] The gas-phase equilibrium ratio of the (1,2) and (2,3) constitutional isomers of the *sec*-butyraldehyde enolate anion (*s*-$C_4H_7O^-$) was measured through quadrupole mass analysis.[16] The relative stabilities of the anions and radicals which have been observed have been attributed to effects such as steric hindrance upon substitution of alkyl groups for the hydrogens in vinoxy, hyperconjugation between substituted groups and the π system in the CCO moiety, and changes in polarizability depending upon the position of substitution.

The current study uses the photodetachment photoelectron spectra of enolate anions to examine the electronic structure of enolate anions and radicals. As in the vinoxy radical, the A($^2A'$) states of the substituted enolates have not been previously characterized. The A($^2A'$) ← X($^1A'$) and X($^2A''$) ← X($^1A'$) transitions have been measured at 355 nm in this work. The adiabatic electron affinities (AEA's) and separation energies of X and A states of the radicals (T_0's) of the substituted species were obtained from the photoelectron spectra and compared. The trends observed in the energetics indicate that both through-bond and through-space interactions of the molecular orbitals in the CCO moiety with the substituent groups affect the relative stabilities of the enolate anion and the low-lying electronic states of the radical. High-level ab initio calculations and Franck−Condon factor (FCF) simulations of the photoelectron spectra were carried out and provided insight into the effects of substitution.

2. Experimental Section

The fast-ion-beam photoelectron spectrometer used in these experiments has been described in detail.[17] A 10% mixture of N_2O in Ar was bubbled through *n*-propanol, 2-propanol, *n*-butanol, *sec*-butanol, or isobutanol (all Fisher, 99+%) at room temperature and produced the corresponding enolate anion in a pulsed discharge ion source.[18] The anions were cooled in a supersonic expansion, and the mass-selected beam at *m*/*e* 57 or 71 was accelerated to 3 keV and crossed with the linearly polarized third harmonic (354.8 nm, 3.494 eV) of a Nd:YAG laser. The electric vector of the laser was oriented parallel to the face of the photoelectron detector. The time-of-flight and position of arrival of the photodetached electrons was recorded by a large-solid-angle time- and position-sensitive detector, yielding the laboratory energy and recoil angle for each photoelectron. After the electron velocity was corrected for the Doppler shift induced by the fast ion beam, the electron kinetic energy in the center of mass frame (eKE) was calculated. The spectrometer was calibrated by photodetachment of O^- and NO^- as described previously.[6] The experimental resolution in eKE was determined to be $\Delta E_{fwhm}/E \sim 4\%$. No evidence for dissociation of the neutral radicals was observed.

3. Calculations

High-level ab initio geometry and frequency calculations were performed with Gaussian 98[19] on the Cray T90 at the San Diego Supercomputer Center (SDSC) in order to aid in the interpretation of the experimental photoelectron spectra. The geometries of the *n*-propionaldehyde (*n*-C_3H_5O), *n*-butyraldehyde (*n*-C_4H_7O), and isobutyraldehyde (*i*-C_4H_7O) enolate anions and radicals were optimized at the CASSCF level. For the species subsequently used in the Franck−Condon factor calculations, the ab initio structural parameters are displayed in Table 1. The normal vibrational modes are given in the Supporting Information. The multireference method was presumed to be necessary since it was required for the calculations previously performed on vinoxide and the vinoxy radicals.[6] The orbitals chosen for the active space were the same as those chosen for vinoxide and the vinoxy radicals. In order of increasing energy, they are the bonding CCO π(a″) orbital, the oxygen σ_{2px}(a′) orbital, and the nonbonding and antibonding CCO π(a″) orbitals. Interaction of the π system with the neighboring a″ CH σ bonds was not sufficient to prevent geometry optimization. The Pople valence triple-ζ basis set including diffuse and polarization functions (6-311++G**) was used to perform the geometry optimizations and normal-mode analysis.[20] The diffuse functions are required to correctly compute the absolute energy of the anion.[21] Single-point CASSCF-MP2 calculations were performed on the optimized geometries to include dynamic correlation in the absolute energies.[22] The CASSCF and CASSCF-MP2 absolute energies corrected by zero point energies are also given in the Supporting Information. The measured experimental energetics are compared to the ab initio results as well as previous experimental values in Table 2. Since the perturbative energies are not bound by the exact solution to the wave function, the agreement between the experimental and calculated energetics varies.

Attempts were also made to calculate the geometries and frequencies of acetone enolate (*i*-C_3H_5O) and *sec*-butyraldehyde enolate (*s*-$C_4H_7O^-$). The geometry of the A($^2A'$) state of these enolates did not optimize using the CASSCF method with the active space mentioned above. This may have been due to the difficulty of excited state ab initio calculations. However, it is also possible that the choice of active space is not correct for enolates with an alkyl substitution on the carbonyl carbon. The active space was varied, but no combination of eight or fewer orbitals could be found for which all three electronic states would optimize. The X($^1A'$) and X($^2A''$) states of *i*-C_3H_5O optimized using the original four orbitals and the normal-mode frequencies were calculated for the sake of comparison of the electronic structures with *n*-C_3H_5O.

Table 1. Structures of *n*-Propionaldehyde and *n*-Butyraldehyde Enolate Anions and Radicals Calculated with the CASSCF Method and the 6-311++G** Basis Set[a]

	n-propionaldehyde			*n*-butyraldehyde		
	X($^1A'$)	X($^2A''$)	A($^2A'$)	X($^1A'$)	X($^2A''$)	A($^2A'$)
C_1-C_2	1.376	1.437	1.334	1.380	1.436	1.334
	1.378	1.440	1.335	–	–	–
C_2-C_3	1.508	1.496	1.504	1.504	1.499	1.506
	1.507	1.495	1.505	–	–	–
C_3-C_4	–	–	–	1.539	1.533	1.530
	–	–	–	–	–	–
C_1-O	1.256	1.218	1.347	1.249	1.218	1.347
	1.258	1.218	1.346	–	–	–
$\angle C_2C_1O$	130.2	123.2	124.4	130.3	123.3	124.5
	129.8	123.8	125.1	–	–	–
$\angle C_1C_2C_3$	123.3	123.5	123.3	123.2	123.6	123.3
	123.3	123.4	125.5	–	–	–
$\angle C_2C_3C_4$	–	–	–	115.0	112.9	112.8
	–	–	–	–	–	–

[a] Atom labels in Figure 4a. Bond lengths in angstroms, bond angles in degrees. (*E*) isomer listed first, (*Z*) isomer second.

(16) Chyall, L. J.; Brickhouse, M. D.; Schnute, M. E.; Squires, R. R. *J. Am. Chem. Soc.* **1994**, *116*, 8681−8690.

(17) Zengin, V.; Persson, B. J.; Strong, K. M.; Continetti, R. E. *J. Chem. Phys.* **1996**, *105*, 9740−9747.

(18) Osborn, D. L.; Leahy, D. J.; Cyr, D. R.; Neumark, D. M. *J. Chem. Phys.* **1996**, *104*, 5026−5039.

(19) Frisch, M. J.; Trucks, G. W.; Schlegel, H. B.; Scuseria, G. E.; Robb, M. A.; Cheeseman, J. R.; Zakrewski, V. G.; Montgomery, J. A.; Stratmann, R. E.; Burant, J. C.; Dapprich, S.; Millam, J. M.; Daniels, A. D.; Kudin, K. N.; Strain, M. C.; Farkas, O.; Tomasi, J.; Barone, V.; Cossi, M.; Cammi, R.; Mennucci, B.; Pomelli, C.; Adamo, C.; Clifford, S.; Ochterski, J.; Petersson, G. A.; Ayala, P. Y.; Cui, Q.; Morokuma, K.; Malick, D. K.; Rabuck, A. D.; Raghavachari, K.; Foresman, J. B.; Cioslowski, J.; Ortiz, J. V.; Stefanov, B. B.; Liu, G.; Liashenko, A.; Piskorz, P.; Komaromi, R.; Gomperts, R.; Martin, R. L.; Fox, D. J.; Keith, T.; Al-Laham, M. A.; Peng, C. Y.; Nanayakkara, A.; Gonzalez, C.; Challacombe, M.; Gill, P. M. W.; Johnson, B. G.; Chen, W.; Wong, M. W.; Andres, J. L.; Head-Gordon, M.; Replogle, E. S.; Pople, J. A. *Gaussian 98*; Gaussian, Inc.: Pittsburgh, 1998.

(20) Krishnan, R.; Binkley, J. S.; Seeger, R.; Pople, J. A. *J. Chem. Phys.* **1980**, *72*, 650−654.

(21) Clark, T.; Chandrasekhar, J.; Spitznagel, G. W.; von Rague Schleyer, P. *J. Comput. Chem.* **1983**, *4*, 294−301.

(22) McDouall, J. J. W.; Peasley, K.; Robb, M. A. *Chem. Phys. Lett.* **1988**, *148*, 183−189.

Table 2. Relative Experimental, CASSCF, and CASSCF-MP2 Energies (in eV) of C_2H_3O, C_3H_5O, and C_4H_7O Enolate Anions and Radicals

		exptl[a]	exptl	CASSCF	CASPT2
AEA	C_2H_3O	1.795 ± 0.015[b]	–	0.14	1.82
AEA	(*E*)-*n*-C_3H_5O	1.619 ± 0.007[c]	1.59 ± 0.02	−0.10	1.49
AEA	(*Z*)-*n*-C_3H_5O	1.73 ± 0.01[c]	1.76	−0.05	1.54
AEA	(*E*)-*n*-C_4H_7O	1.670 ± 0.052[d]	1.64 ± 0.02	−0.02	1.79
AEA	(*Z*)-*n*-C_4H_7O			–	–
AEA	*i*-C_3H_5O	1.758 ± 0.019[e]	1.76 ± 0.02	–	–
AEA	(2,3)-*s*-C_4H_7O	1.674 ± 0.052[d]	1.49 ± 0.02	–	–
AEA	(1,2)-*s*-C_4H_7O	1.747 ± 0.056[d]	1.76 ± 0.02	–	–
AEA	*i*-C_4H_7O	–	1.38 ± 0.02	−0.16	1.39
T_0	C_2H_3O	1.015 ± 0.015[b]	–	0.87	0.92
T_0	(*E*)-*n*-C_3H_5O	–	1.19 ± 0.02	1.03	1.19
T_0	(*Z*)-*n*-C_3H_5O	–	0.99 ± 0.02	1.09	1.24
T_0	(*E*)-*n*-C_4H_7O	–	1.19 ± 0.02	1.05	1.14
T_0	(*Z*)-*n*-C_4H_7O			–	–
T_0	*i*-C_3H_5O	–	1.01 ± 0.02	–	–
T_0	(2,3)-*s*-C_4H_7O	–	1.25 ± 0.02	–	–
T_0	(1,2)-*s*-C_4H_7O	–	0.98 ± 0.02	–	–
T_0	*i*-C_4H_7O	–	1.36 ± 0.02	1.17	1.38

[a] Previous experimental results. [b] Reference 6. [c] Reference 10. [d] Reference 7. [e] Reference 9.

The Franck−Condon factor (FCF) calculations that were used to simulate the *n*-$C_3H_5O^-$ and *n*-$C_4H_7O^-$ photoelectron spectra have been described previously.[6] Since the FCF simulation of the *i*-$C_4H_7O^-$ photoelectron spectrum did not provide insight into the effect of the alkyl substitutions, it is not presented here. The intensity of a transition between vibrational modes of the enolate anion and radical, expressed as the square of the overlap integral between vibrational wave functions, was evaluated by using the generating function for a multidimensional harmonic oscillator, neglecting anharmonic effects.[23,24] Chen and coworkers developed an algorithm to calculate FCFs that implements the generating function method and includes the Duchinsky effect for polyatomic molecules.[25] The algorithm uses the structural and normal mode information from the ab initio results to obtain the transition energies. The standard coordinates employed in Gaussian 98 to report molecular properties place the center of nuclear charge at the origin.[26] To prevent false overlap in the FCF calculations, the vector from the center of nuclear charge to the center of mass was used to align the two species, the center of mass was placed at the origin and the molecular coordinates were recalculated prior to the FCFs. The transition energies were converted into electron kinetic energies and the corresponding intensities were convoluted with Gaussian functions to simulate the experimental resolution. The anion temperature was assumed to be 0 K, since efficient cooling was observed in vinoxide, but FCF calculations at higher anion temperatures were also performed to determine the anion temperatures at which hot band contributions might become significant (500 K in *n*-$C_3H_5O^-$ and 700 K in *n*-$C_4H_7O^-$). The simulated spectra are compared to the experimental photoelectron spectra of *n*-$C_3H_5O^-$ and *n*-$C_4H_7O^-$ to aid in the interpretation of the observed structure.

4. Results

All of the enolate anions undergo photodetachment to both the ground and first excited states of the corresponding neutral radical at 355 nm. The photoelectron spectra in Figures 1, 2, and 3 show photoelectrons detected in concidence with the stable neutral photofragment. The FCF-simulated contributions of the (*E*) and (*Z*) stereoisomers of *n*-$C_3H_5O^-$ are shown in Figure 1, parts a and b, respectively, and the sum of the contributions is compared with the experimental spectrum in Figure 1c. The structures of the two stereoisomers are shown as well. It is

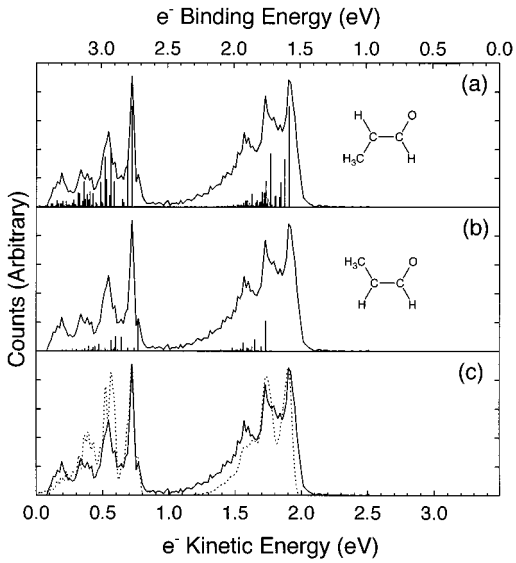

Figure 1. Simulated and experimental photoelectron spectra of *n*-propionaldehyde enolate anion, *n*-$C_3H_5O^-$. The simulated relative contributions of the (*E*) and (*Z*) stereoisomers are compared to the experimental spectrum in parts a and b, respectively. The summed contributions are compared to the experimental spectrum in part c. The convolution of the simulated spectrum is displayed as a dashed line in part c.

presumed that the (*E*) and (*Z*) stereoisomers both contribute to the *n*-propionaldehyde enolate photoelectron spectrum since they have been observed separately. It was assumed that the (*E*) stereoisomer dominates the photoelectron spectrum measured in this study for two reasons. First, previous studies performed on mixtures of the two stereoisomers primarily exhibit the features observed in the (*E*) stereoisomer.[7−9] Second, in the parent alcohol, it is likely that it is sterically favorable for the methyl group attached to the α carbon to be oriented trans to the CO bond. This conformation preferentially forms the (*E*) stereoisomer of the enolate anion. Figure 2 shows the structures and FCF-simulated contribution of the (*E*) stereoisomer to the *n*-$C_4H_7O^-$ spectrum. Although both the (*E*) and (*Z*) stereoisomers of *n*-butyraldehyde enolate are presumably formed in the pulsed discharge ion source, the individual contributions to the photoelectron spectrum could not be distinguished. It is again reasonable to expect that the (*E*) stereoisomer will dominate the anion population as in *n*-propionaldehyde enolate, since steric considerations indicate that the ethyl group attached to

(23) Sharp, T. E.; Rosenstock, H. M. *J. Chem. Phys.* **1964**, *41*, 3453−3463.
(24) Warshel, A.; Karplus, M. *Chem. Phys. Lett.* **1972**, *17*, 7−14.
(25) Chen, P. in *Unimolecular and Bimolecular Reaction Dynamics*; Ng, C. Y., Baer, T., Powis, I., Eds.; Wiley & Sons: Chichester, 1994; pp 371−425.
(26) Foresman, J. B.; Frisch, A. in *Exploring Chemistry with Electronic Structure Methods*, 2nd ed.; Gaussian, Inc.: Pittsburgh, PA, 1996; p 16.

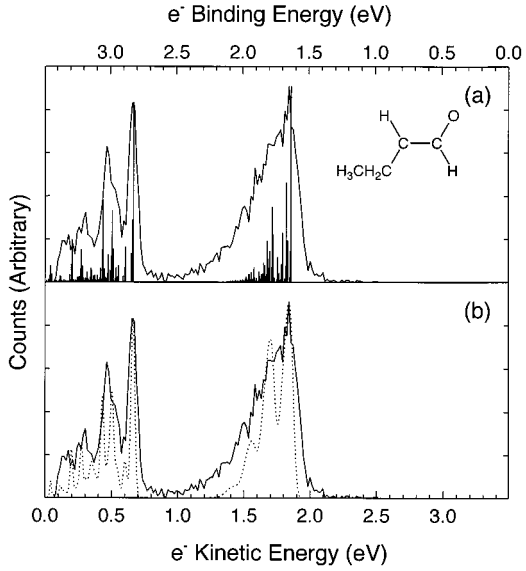

Figure 2. Simulated and experimental photoelectron spectra of *n*-butyraldehyde enolate, *n*-$C_4H_7O^-$. The simulated stick spectrum of the (*E*) stereoisomer is compared to the experimental spectrum in part a. The convoluted simulation, displayed as a dashed line, is compared to the experimental spectrum in part b.

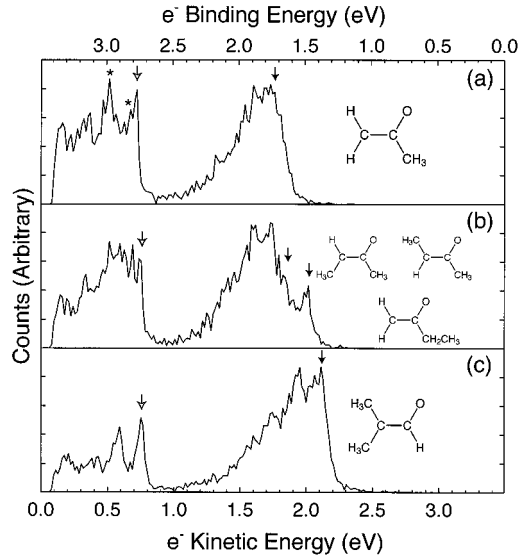

Figure 3. Photoelectron spectra of *i*-$C_3H_5O^-$ (a), *s*-$C_4H_7O^-$ (b), and *i*-$C_4H_7O^-$ (c). Filled arrows indicate adiabatic electron affinity (AEA) determinations while open arrows indicate the determination of the separation energy between X and A electronic states (T_0). The structures are shown as well. Conformational isomers clockwise from the upper left in part b: (*E*)-(2,3)-*s*-$C_4H_7O^-$, (*Z*)-(2,3)-*s*-$C_4H_7O^-$, and (1,2)-*s*-$C_4H_7O^-$.

the α carbon is oriented trans to the CO bond. The structures and photoelectron spectra of the enolates formed from secondary and branched parent alcohols, *i*-$C_3H_5O^-$, *s*-$C_4H_7O^-$, and *i*-$C_4H_7O^-$, are shown in Figure 3. In Figure 4, ab initio molecular orbitals and structures for *n*-C_3H_5O and *i*-C_3H_5O and atom labels are displayed to assist in the interpretation of the photoelectron spectra and energetics. The relative stabilities of the X(^{1}A′) state of the anion and the A(^{2}A′) state of the radical for all species are compared in Figure 5.

5. Discussion

In section A, the individual contributions of the (*E*) and (*Z*) stereoisomers to the photoelectron spectrum of *n*-propionaldehyde enolate (*n*-$C_3H_5O^-$) are contrasted in detail and interpreted with the aid of the FCF simulations. In section B, the features of the *n*-butyraldehyde enolate (*n*-$C_4H_7O^-$) photoelectron spectrum are compared to FCF simulations. In sections C, D, and E respectively, the acetone (*i*-$C_3H_5O^-$), *sec*-butyraldehyde (*s*-$C_4H_7O^-$), and isobutyraldehyde (*i*-$C_4H_7O^-$) enolate photoelectron spectra are discussed. Finally, the photoelectron spectra of each of the $C_3H_5O^-$ and $C_4H_7O^-$ enolates are compared to vinoxide to determine the effects of alkyl substitution on the energetics and vibronic structure.

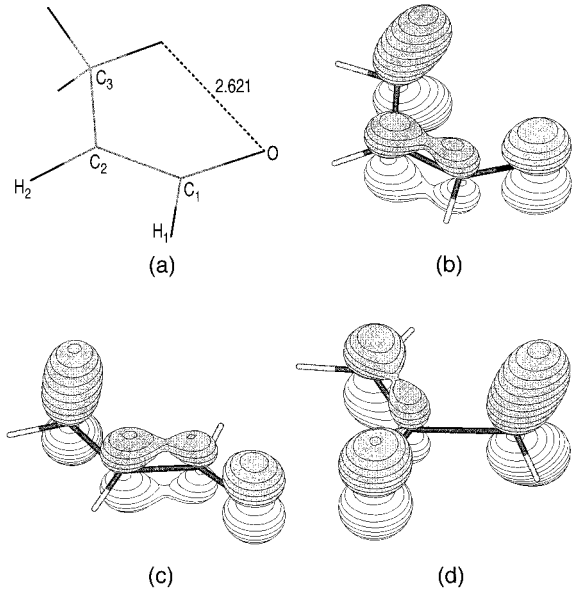

Figure 4. Possible interactions of the doubly occupied CCO π bonding and nonbonding orbitals with the methyl group in the X(^{1}A′) state of the isomers of $C_3H_5O^-$. The hydrogen bond in the cis conformation (a) and molecular orbital configuration in the trans conformation (b) of (*Z*)-*n*-$C_3H_5O^-$ are shown. The (*E*)-*n*-$C_3H_5O^-$ and *i*-$C_3H_5O^-$ molecular orbital configurations are shown in parts c and d, respectively. The molecular orbitals were generated from Gaussian 98 calculations with Molden.[30]

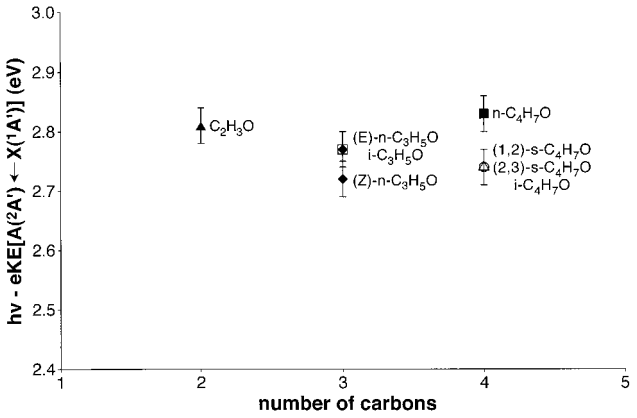

Figure 5. An energetics comparison of the two-, three-, and four-carbon enolates. The values of $h\nu$ − eKE[A(^{2}A′), $v' = 0 \leftarrow$ X(^{1}A′), $v' = 0$] in eV for the identified structural isomers, constitutional isomers, and stereoisomers are plotted against the number of carbons in the enolate, illustrating the small variation observed in the relative energetics of the anion and the first excited states of the enolate radicals.

A. *n*-Propionaldehyde Enolate (*n*-$C_3H_5O^-$). In the *n*-propionaldehyde enolate spectrum shown in Figure 1, neither the (*E*) nor the (*Z*) FCF simulation alone could account for most of the complex vibronic structure observed in the X(^{2}A″) ← X(^{1}A′) transition. A mixture of 77% (*E*) and 23% (*Z*) gave the

best fit of the FCF simulation to the experimental spectrum. The vibrational transitions to $v' = 1$ in the C_1C_2 stretch (1134 cm^{-1}) and the C_1O stretch (1518 cm^{-1}) in the (*E*) stereoisomer are the most intense. The best fits of the (*E*) and (*Z*) stereoisomer spectra to the experimental spectrum were obtained with the adiabatic electron affinities (AEA's) of 1.59 and 1.76 eV, respectively. The peak at eKE = 1.90 eV has been assigned to the 0−0 transition in the (*E*) stereoisomer. The contribution of the 0−0 transition in the (*Z*) stereoisomer was attributed to the feature at eKE = 1.73 eV because the (*E*) stereoisomer does not account for it. Since the determination of the (*Z*) stereoisomer AEA in this study is tentative, the value determined by Brauman and co-workers is deemed preferable.[10] The (*E*) stereoisomer AEA agrees with the previously determined value, as shown in Table 2. The trend in the experimental AEA's is reflected by the CASPT2 AEA's, though the ab initio values differ quantitatively (Table 2).

In the portion of the photoelectron spectrum corresponding to the $A(^2A') \leftarrow X(^1A')$ electronic transition, it is difficult to determine the relative contributions of the (*E*) and (*Z*) isomers. The best fit of the simulated to experimental spectra is obtained when the peaks at eKE = 0.72 and 0.77 eV correspond to the 0−0 transitions for (*E*) and (*Z*) stereoisomers, respectively. The relative intensities of these peaks corroborates the fractional contributions attributed to the (*E*) and (*Z*) stereoisomers to the mixture. The peak at eKE = 0.77, with a spacing of 323 cm^{-1} from the 0−0 transition, could be due to a hot band. However, significant contributions from hot bands were not calculated in either stereoisomer FCF simulation unless an anion temperature of 500 K or greater was assumed. Additionally, there are no clearly resolved hot bands in the $X(^2A'') \leftarrow X(^1A')$ electronic transition. The peak assignment yields separation energies between the $X(^2A'')$ and $A(^2A')$ states (T_0) of 1.19 ± 0.02 and 0.99 ± 0.02 eV for the (*E*) and (*Z*) stereoisomers, respectively.

In general, the vibrational excitation in the FCF simulation for the $A(^2A') \leftarrow X(^1A')$ electronic transition exceeds the experimentally observed excitation. The same effect was observed in the FCF simulation for the $A(^2A') \leftarrow X(^1A')$ transition in $C_2H_3O^-$.[6] The most intense transitions occur in the $C_1C_2C_3$ in-plane bend (282 cm^{-1}), the OC_1H_1 in-plane bend (1274 cm^{-1}), and the C_1C_2 stretch (1633 cm^{-1}) of the (*E*) stereoisomer. The excitation in the $C_1C_2C_3$ bend is surprising, since this bond angle does not change much from the $X(^1A')$ state to the $A(^2A')$ state (Table 1). Since the change in C_1C_2O bond angle is significant, excitation in the C_1C_2O bend (498 cm^{-1}) was expected. However, the simulation did not predict it. The feature observed experimentally at eKE = 0.64 eV, for which the simulation does not entirely account, may be due to excitation in the C_1C_2O bend. The position of the feature relative to the 0−0 transition and the intensity are similar to the feature attributed to the C_1C_2O bend in the vinoxide spectrum.[6] It is reasonable to expect considerable excitation in the OC_1H_1 in-plane bend and the C_1C_2 stretch because of the changes in geometry as seen in Table 1. Moderate excitation is also predicted for the C_2C_3 stretch (1076 cm^{-1}) and CO stretch (1083 cm^{-1}). These features are not distinguishable in the experimental photoelectron spectrum with the intensity predicted by the simulation.

The methyl substitution on the α carbon significantly affects the relative stability of the $X(^1A')$ *n*-C_3H_5O enolate anion and $X(^2A'')$ radical stereoisomer. The methyl group has an inductive (through-bond) electron-donating effect on the π system. In the $X(^1A')$ anion, the CCO π orbitals are filled, so electron donation is unfavorable. In the $X(^2A'')$ radical, the CCO π nonbonding orbital is singly occupied, so electron donation is favorable. The net effect is a reduction of the AEA from the one measured for the vinoxy radical.[6] The AEA of the (*E*)-*n*-C_3H_5O stereoisomer indicates that the inductive effect dominates. However, the AEA of (*Z*)-*n*-C_3H_5O is not shifted as much from that of vinoxy, indicating that the spatial positioning of the CH σ bonds with respect to the occupied CCO π orbitals also affects the relative $X(^2A'')-X(^1A')$ stability.

In $X(^1A')$ *n*-$C_3H_5O^-$, the electron density in the HOMO (the CCO π nonbonding orbital) is localized over the oxygen in both stereoisomers. Some electron density in the HOMO shifts to the α carbon when an electron is removed to form the $X(^2A'')$ state of the radical. In the (*Z*) stereoisomer, the methyl group could be oriented with one of the CH σ bonds in the plane either cis or trans to the CH bond on the carbonyl carbon, without breaking C_s symmetry. The distance between the H in this a′ CH σ bond and the O in the cis conformation is 2.62 Å (Figure 4a), giving rise to the possibility of intramolecular hydrogen bonding. The typical strength of a hydrogen bond is between 2 and 15 kcal/mol[27] and the difference between the AEA's in the (*E*) and (*Z*) stereoisomers is 2.6 kcal/mol (according to the previously determined values). In the trans conformation, the two electrons in the a″ CH σ bonding orbital can interact with the two electrons in the HOMO and also the two electrons in the CCO π bonding orbital through space, as shown in Figure 4b. Although the terminal carbon is not bonded to the oxygen, the planar, conjugated, 6 electron system fulfills most of the Hückel conditions for aromaticity,[28] which would result in stabilization of the anion. The removal of an electron from the HOMO breaks the aromaticity, making photodetachment less energetically favorable. The CASSCF calculations on the $X(^2A'')$ state indicate that the cis conformation corresponds to a minimum on the potential energy surface while the trans does not, in agreement with previous calculations.[14] Either conformation could account for stabilization of the $X(^1A')$ state of the anion with respect to the $X(^2A'')$ state in the (*Z*) stereoisomer. In contrast, the methyl group in the (*E*) stereoisomer anion cannot interact with the a′ oxygen lone pair (not shown) or the a″ HOMO through space as shown in Figure 4c, so neither hydrogen bonding nor aromatic stabilization affect the energetics. Energetic considerations dictate that the (*Z*) stereoisomer should dominate the anion population. However, the observed dominance of the (*E*) stereoisomer indicates that the formation of the (*E*) stereoisomer anion from the parent alcohol is sterically favorable, as discussed previously in the Results section.

The energy difference between the $X(^1A')$ anion and the $A(^2A')$ radical is 2.81 eV in vinoxy and 2.77 and 2.72 eV in the (*E*) and (*Z*) stereoisomers of *n*-C_3H_5O, respectively (Figure 5). This shows that the $X(^1A')-A(^2A')$ relative stability is not strongly affected by the methyl group. The experimental energetics, corroborated by the CASSCF calculations, indicate that the change in the electronic structure from $X(^1A')$ to $A(^2A')$ is minimal. In the (*E*) stereoisomer and the trans conformation of the (*Z*) stereoisomer, the lack of energetic perturbation is to be expected, since the a′ O σ_{2p} orbital from which the electron is photodetached does not interact with the a″ π and the a′ and a″ CH σ bonding orbitals. However, removing an electron from the a′ O σ_{2p} orbital would disrupt the hydrogen bond in the cis conformation of the (*Z*) stereoisomer and decrease the relative $X(^1A')-A(^2A')$ stability. This may explain the greater reduction

(27) Scheiner, S. *Hydrogen Bonding: A Theoretical Perspective*; Oxford University Press: New York, 1997.

(28) Dewar, M. J. S. *The Molecular Orbital Theory of Organic Chemistry*; McGraw-Hill, Inc.: New York, 1969.

in the energy difference between X(^{1}A′) and A(^{2}A′) in the (*Z*) stereoisomer.

B. *n*-Butyraldehyde Enolate (*n*-$C_4H_7O^-$). The FCF simulation of the (*E*) stereoisomer of *n*-butyraldehyde enolate alone accounts for much of the vibrational structure observed in the spectrum in Figure 2. The intense peaks at eKE = 1.84 and 0.66 eV have been assigned to the 0−0 vibrational transitions in the X(^{2}A″) ← X(^{1}A′) and A(^{2}A′) ← X(^{1}A′) electronic transitions, respectively, without assigning them to either stereoisomer. The experimental AEA of 1.64 ± 0.02 eV is in agreement with the previously determined value (Table 2). The calculated CASPT2 AEA for the (*E*) stereoisomer differs significantly from the experimental AEA.

Specific vibrational features in the portion of the photoelectron spectrum corresponding to the X(^{2}A″) ← X(^{1}A′) transition could not be assigned. The length of the leading edge and two small peaks at eKE's higher than 1.84 eV could be due to hot bands, although this seems unlikely since significant hot band contributions are not calculated in the FCF simulation unless an anion temperature of 700 K or greater is assumed, and efficient cooling has been observed in the smaller enolate anions. Instead, these features may be evidence of the contribution of the (*Z*) stereoisomer. In the portion of the experimental photoelectron spectrum corresponding to the A(^{2}A′) ← X(^{1}A′) transition, vibrational transitions with greater intensity than the simulation are visible at eKE = 0.60 and 0.47 eV. The unknown mixture of (*E*) and (*Z*) stereoisomers prevents the assignment of specific vibrational modes. The transition energies and intensities are comparable to those observed in the A(^{2}A′) ← X(^{1}A′) vinoxy spectrum, which suggests that these features are due to activity in the CCO bending and CC stretching modes.

Once again, it is found that the X(^{1}A′)−X(^{2}A″) relative stability is significantly perturbed by alkyl substitution on the α carbon, but the X(^{1}A′)−A(^{2}A′) relative stability is not. The ethyl group, like the methyl group in *n*-C_3H_5O, has an inductive electron-donating effect that reduces the AEA from that of vinoxy. The CASSCF geometry optimizations of the (*E*) stereoisomer anion and radicals converged to structures far from C_s symmetry, with the CH_3 group angled out of the plane defined by the OC_1H_1 bond angle. The C_3C_4 σ bonding orbital could potentially interact with the π system in this configuration. Additionally, in the (*Z*) stereoisomer anion, one of the hydrogens on the β carbon could interact with the a′ O σ_{2p} lone pair. Separate experimental studies of the (*E*) and (*Z*) will be necessary to analyze the through-bond and through-space interactions governing the energetics in detail.

C. Acetone Enolate (*i*-$C_3H_5O^-$). The energetics of acetone enolate are similar to those of vinoxy although the structure in the photoelectron spectrum differs significantly. The broadened structure in the portion of the photoelectron spectrum in Figure 3a corresponding to the X(^{2}A″) ← X(^{1}A′) transition precludes assignment of the vibrational features. The 0−0 transition is assigned to the leading edge at eKE = 1.73 eV. The measured AEA of 1.76 ± 0.02 eV is in agreement with the previous experimental value shown in Table 2. The peak spacings in the A(^{2}A′) ← X(^{1}A′) transition as well as the measured T_0 of 1.01 ± 0.02 eV are nearly the same as those measured in the vinoxide photoelectron spectrum. The peak intensities are higher in acetone enolate and the ratio of peak heights is changed from vinoxide as well. The most intense peaks in the vinoxy spectrum corresponding to the A(^{2}A′) ← X(^{1}A′) transition were assigned to $v' = 1$ in ν_4 (CC stretch, 1580 cm^{-1}), ν_5 (CH_2 scissors, 1350 cm^{-1}), and ν_9 (CCO bend, 460 cm^{-1}). The transitions at 400 and 1700 cm^{-1} (peaks marked with asterisks in Figure 3a) probably arise from analogous $v' = 1$ excitations in the CCO or CCC bending and CC stretching modes in the A(^{2}A′) state of acetone enolate. The less intense transitions may be due to combination bands and additional quanta in these modes, as they are in vinoxy.

The acetone enolate spectrum shows that methyl substitution on the carbonyl carbon of vinoxy perturbs the vibronic structure observed in the photoelectron spectrum, particularly in the A(^{2}A′) ← X(^{1}A′) transition, though the energetics remain similar. The methyl group may have an inductive electron-donating effect, thereby reducing the AEA. This effect is weaker than in *n*-C_3H_5O, since very little electron density in the HOMO is located over the carbonyl carbon. The methyl group could be oriented with one of the CH σ bonds either cis (Figure 4d) or trans to the CO bond in the anion without breaking the C_s symmetry. In both conformations the distances (∼2.5 Å from the CASSCF optimized geometries) between the oxygen and the hydrogens on the methyl group could give rise to intramolecular hydrogen bonding that would stabilize the anion. The combination of through-bond and through-space effects may account for the slight lowering of the electron affinity relative to vinoxy and the broadened structure observed in the photoelectron spectrum. As in both stereoisomers of *n*-C_3H_5O, the X(^{1}A′)−A(^{2}A′) relative stability in *i*-C_3H_5O is not strongly affected by the methyl group. The perturbation of the vibronic structure in the A(^{2}A′) ← X(^{1}A′) transition by the addition of the methyl group indicates the participation of other through-bond or through-space interactions. The convergence failure of the CASSCF calculations with the (5,4) active space indicated that the orbital interactions were altered when the methyl group was substituted on the carbonyl carbon compared to vinoxide. The geometry of the A(^{2}A′) state of acetone enolate optimized with the addition of the unoccupied a′ O σ_{3p} orbital to the active space. The spread of electron density over the oxygen atom may induce the observed changes in peak intensity in the experimental photoelectron spectrum.

D. *sec*-Butyraldehyde Enolate (*s*-$C_4H_7O^-$). The highly perturbed structure in the *sec*-butyraldehyde enolate photoelectron spectrum shown in Figure 3b can be accounted for by the two possible constitutional isomers of *sec*-butyraldehyde enolate, which have been observed previously in approximately equal abundance in the gas phase.[16] Substitution of an ethyl group for the hydrogen on the carbonyl carbon in vinoxy yields the (1,2) isomer. Two methyl group substitutions, one on the carbonyl carbon and another in either the (*E*) or (*Z*) position on the α carbon in vinoxy produce the two stereoisomers of (2,3)-*s*-C_4H_7O.

The region of the photoelectron spectrum corresponding to the X(^{2}A″) ← X(^{1}A″) electronic transition has two sharp transitions at eKE = 1.73 and 2.00 eV. The (1,2)-*s*-C_4H_7O isomer is analogous to *i*-C_3H_5O. Since the methyl group on the carbonyl carbon perturbed the electronic structure only slightly, it is reasonable to expect that the effect of the ethyl group would be similarly minor. Therefore, the peak at lower eKE has been assigned to the 0−0 transition in this isomer, yielding an AEA of 1.76 ± 0.02 eV. This peak is more intense than the peak at higher eKE, though the two conformational isomers are presumed to be equally abundant. The enhancement of the peak at eKE = 1.73 eV may be explained by the presence of the (*Z*)-(2,3)-*s*-C_4H_7O stereoisomer. Substitution of a methyl group on the carbonyl carbon of (*Z*)-*n*-C_3H_5O yields this stereoisomer. Consistent with the effect observed in *i*-C_3H_5O, this substitution does little to perturb the electronic structure, therefore the aromatic stabilization is maintained. Additionally, the shift of

the AEA in (Z)-*n*-C_3H_5O from that of vinoxy is slight, therefore the shift for (*Z*)-(2,3)-*s*-C_4H_7O is expected to be small.

The peak at higher eKE is assigned to the 0−0 transition in the (2,3)-*s*-C_4H_7O constitutional isomer, yielding an AEA of 1.49 ± 0.02 eV. This peak is likely due to the (*E*) stereoisomer. Several factors may contribute to the large shift from the AEA of vinoxy in this isomer, which can be viewed as (*E*)-*n*-C_3H_5O with a methyl group substituted on the carbonyl carbon. The methyl group on the α carbon may inductively donate electrons to the filled π system in the anion, thereby destabilizing it with respect to the radical. No stabilization by through-space interaction of the methyl group on the α carbon with the filled a″ π system or the a′ oxygen σ lone pair can occur in the anion. The isomer may be further destabilized by steric hindrance, since both methyl groups are in the plane of symmetry on the same side of the CC bond (Figure 4b).

The structure in the region of the photoelectron spectrum corresponding to the $A(^2A') \leftarrow X(^1A'')$ electronic transition cannot be easily deconvoluted. The complex structure is likely due to the superposition of two slightly energetically shifted spectra corresponding to the (1,2) and (2,3) constitutional isomers. However, the first sharp peak at eKE = 0.75 eV is assigned to the 0−0 transition in both isomers. Even with the uncertainty in the value of T_0, the $X(^1A')-A(^2A')$ relative stability (2.74 eV compared to 2.81 eV in C_2H_3O) does not appear to be strongly affected by the substitutions in *s*-C_4H_7O as shown in Figure 5.

E. Isobutyraldehyde Enolate (*i*-$C_4H_7O^-$). Although the structure in the photoelectron spectrum of isobutyraldehyde enolate in Figure 3c is similar to that of vinoxy, there is a large change in the energetics. Specifically, the 0−0 transition in the portion of the photoelectron spectrum corresponding to the $X(^2A'') \leftarrow X(^1A')$ electronic transition in *i*-C_4H_7O occurs at eKE = 2.11 eV, yielding an AEA of 1.38 ± 0.02 eV. Substitution of methyl groups for both hydrogens on the α carbon in vinoxy gives the structure of *i*-C_4H_7O. Summing the effects of the two possible single substitutions, which form the (*E*) and (*Z*) stereoisomers of *n*-C_3H_5O, does not accurately predict the effects of the double substitution. The reduction in the AEA of *i*-C_4H_7O from that of vinoxy would be expected to equal the sum of the reductions in the AEA's of (*E*) and (*Z*) stereoisomers of *n*-C_3H_5O, or 0.24 ± 0.03 eV, rather than the 0.41 ± 0.03 eV obtained from the experimental results.

The peak at eKE = 0.75 eV has been assigned to the $A(^2A') \leftarrow X(^1A')$ transition, yielding $T_0 = 1.36 \pm 0.02$ eV for *i*-C_4H_7O. The vibronic structure in this portion of the photoelectron spectrum is perturbed from that of vinoxide in both peak positions and intensities. The sharp peak at 0.59 eV may be due to activity in the CO stretching mode, since the CASSCF frequencies indicate that this mode is around 1200 cm^{-1} while the CC stretching mode is near 1800 cm^{-1}. Activity in the CO stretch was expected in vinoxy, due to the significant change in CO bond length from the $X(^1A')$ state of the anion to the $A(^2A')$ state of the radical, but not observed. It is also intriguing that the calculated CASPT2 AEA and T_0 agree well with the experimental energetics. The relative $A(^2A')-X(^1A')$ stability (2.74 eV) is not significantly perturbed by the methyl substitutions on the α carbon. The perturbation of the $X(^1A')-X(^2A'')$ relative stability as well as the changes in vibronic structure indicate that through-bond and through-space interactions of the methyl substituents with the CCO moiety strongly affect the photodetachment processes of this enolate.

6. Conclusion

Photodetachment to the ground and first excited states of the substituted isomers of the three- and four-carbon enolates has been observed at 355 nm. These results have provided the first experimental determination of the excited-state energetics (T_0). Contributions from constitutional isomers and stereoisomers have been observed. The changes in the vibronic structure and energetics from the previously measured photoelectron spectrum of vinoxide indicate the complex effects of through-bond and through-space interactions when alkyl groups are substituted for the hydrogens on vinoxide. Specifically, alkyl substitution on the carbonyl carbon produces larger changes in the vibronic structure while alkyl substitution on the α carbon effects the most change in the energetics.

To further elucidate the effects of through-bond and through-space interactions in enolates, it would be useful to study the constitutional isomers and stereoisomers independently. For example, it has been shown that the (2,3)-*s*-$C_4H_7O^-$ and (1,2)-*s*-$C_4H_7O^-$ constitutional isomers can be produced from trimethylsilyl enol ether precursors.[15] Since photodetachment to the $A(^2A')$ state occurs from a p-like orbital yielding s-wave electrons, it is also possible that threshold photodetachment studies could provide more information on the structures and vibronic activity in these enolates. These studies could be pursued through the use of tunable laser radiation coupled with the recently implemented space-focusing photoelectron imaging assembly.[29]

Acknowledgment. This work was supported by the Chemistry Division of the National Science Foundation under Grant CHE 97-00142. The theoretical research was supported by NSF cooperative agreement ACI-9619020 through computing resources provided by the National Partnership for Advanced Computational Infrastructure at the San Diego Supercomputer Center. We thank Profs. Charles Perrin and Jay Siegel for helpful discussions concerning the enolate energetics.

Supporting Information Available: Ab initio calculations at the CASSCF and CASSCF-MP2 levels of theory (PDF). This material is available free of charge via the Internet at http://pubs.acs.org.

JA0120431

(29) Alconcel, L. S.; Deyerl, H.-J.; DeClue, M.; Continetti, R. E. *J. Am. Chem. Soc.* **2001**, *123*, 3125−3132.

(30) Schaftenaar, G.; Noordik, J. H. *J. Comput. Aided Mol. Des.* **2000**, *14*, 123−134.